THE PROGRADE ORBIT OF EXOPLANET TrES-2b[1]

JOSHUA N. WINN,[2] JOHN ASHER JOHNSON,[3,4] NORIO NARITA,[5] YASUSHI SUTO,[5] EDWIN L. TURNER,[6] DEBRA A. FISCHER,[7]
R. PAUL BUTLER,[8] STEVEN S. VOGT,[9] FRANCIS T. O'DONOVAN,[10] AND B. SCOTT GAUDI[11]

ABSTRACT

We monitored the Doppler shift of the G0 V star TrES-2 throughout a transit of its giant planet. The anomalous Doppler shift due to stellar rotation (the Rossiter-McLaughlin effect) is discernible in the data, with a signal-to-noise ratio of 2.9, even though the star is a slow rotator. By modeling this effect we find that the planet's trajectory across the face of the star is tilted by $-9° \pm 12°$ relative to the projected stellar equator. With 98% confidence, the orbit is prograde.

Subject headings: planetary systems — planetary systems: formation —
stars: individual (GSC 03549−02811, TrES-2) — stars: rotation

1. INTRODUCTION

A small fraction of Sun-like stars have giant planets with orbital periods smaller than about 10 days (Marcy et al. 2005; Udry & Santos 2007). The existence of these planets was a surprise, because it was expected that giant planets would only be found beyond the "snow line," with orbital distances greater than a few astronomical units. Other surprises have come from detailed studies of individual objects. Some are found on highly eccentric orbits (Johnson et al. 2006; Bakos et al. 2007; Maness et al. 2007; Johns-Krull et al. 2008). Some have mean densities that are quite small (Knutson et al. 2007; Mandushev et al. 2007) or large (Sato et al. 2005; Torres et al. 2007) in comparison with Jupiter.

However, in at least one sense, the close-in giant planets have fulfilled prior expectations: they orbit their host stars in the prograde direction, relative to the sense of the stellar rotation. This is true, at least, of the six systems for which measurements of spin-orbit alignment have been reported (Queloz et al. 2000; Wolf et al. 2007; Narita et al. 2007, 2008; Loeillet et al. 2008; Winn et al. 2005, 2006, 2007b). In all of these cases but one, the sky projections of the orbital axis and the stellar rotation axis are observed to be fairly well aligned, with measurement precisions ranging from about $1.5°$–$30°$. The exception is HD 17156, for

which the angle between those axes was found to be $62° \pm 25°$ (Narita et al. 2008). In all of these cases, the measurement technique relies on the Rossiter-McLaughlin (RM) effect, the anomalous Doppler shift that occurs during transits due to stellar rotation (see, e.g., Queloz et al. 2000; Ohta et al. 2005; Giménez 2006; Gaudi & Winn 2007; Winn 2007).

A close alignment between the orbital and rotational axes seems natural because this pattern prevails in the Solar system, and because the angular momenta of the parent star and the planetary orbits presumably derive from the same protostellar disk. However, some theories of planetary migration—proposed to explain how giant planets attain short-period orbits—predict occasionally large misalignments (Chatterjee et al. 2007; Fabrycky & Tremaine 2007; Wu et al. 2007; Nagasawa et al. 2008). These theories, as well as the general history of surprises in this field, provide motivation to continue measuring exoplanetary spin-orbit alignment.

In this paper we present a measurement of the RM effect for the transiting exoplanetary system TrES-2. This system was discovered by O'Donovan et al. (2006). It consists of a planet with a mass of $1.2\,M_{\rm Jup}$ and radius $1.2\,R_{\rm Jup}$ orbiting a G0 V star with a period of 2.5 days (O'Donovan et al. 2006; Holman et al. 2007; Sozzetti et al. 2007). It did not stand out as a promising RM target because the star is relatively faint ($V = 11.4$) and is a slow rotator ($v \sin i_\star = 2.0 \pm 1.5$ km s^{-1}; O'Donovan et al. 2006). On the other hand, the transit occurs at a high impact parameter across the stellar disk ($b = 0.8540 \pm 0.0062$; Holman et al. 2007), a favorable circumstance for this type of measurement (Gaudi & Winn 2007). Furthermore, in our continuing effort to measure the spin-orbit angles for a statistically meaningful number of systems, we do not want to ignore stars with small sky-projected rotation rates. This is because a small value of $v \sin i_\star$ might be caused by a small value of $\sin i_\star$, i.e., there might be a large spin-orbit misalignment. For these reasons, we pursued TrES-2. We describe the new data in § 2, the model that we used to interpret the data in § 3, and the results in § 4.

2. OBSERVATIONS AND DATA REDUCTION

We observed a transit of TrES-2 on UT 2007 April 26 with the Keck I 10 m telescope and the High Resolution Echelle Spectrometer (HIRES; Vogt et al. 1994). We set up the instrument in the same manner that has been used consistently for the California-Carnegie planet search (Butler et al. 1996, 2006). In

[2] Department of Physics, and Kavli Institute for Astrophysics and Space Research, Massachusetts Institute of Technology, Cambridge, MA 02139.

[3] Department of Astronomy, University of California, Mail Code 3411, Berkeley, CA 94720.

[4] Current address: Institute for Astronomy, University of Hawaii, 2226 Woodlawn Drive, Honolulu, HI 96822.

[5] Department of Physics, University of Tokyo, Tokyo 113-0033, Japan.

[6] Princeton University Observatory, Peyton Hall, Princeton, NJ 08544.

[7] Department of Physics and Astronomy, San Francisco State University, San Francisco, CA 94132.

[8] Department of Terrestrial Magnetism, Carnegie Institution of Washington, 5241 Broad Branch Road NW, Washington, D.C. 20015-1305.

[9] UCO/Lick Observatory, University of California at Santa Cruz, Santa Cruz, CA 95064.

[10] California Institute of Technology, 1200 E. California Boulevard, Pasadena, CA 91125.

[11] Department of Astronomy, Ohio State University, 140 West 18th Avenue, Columbus, OH 43210.

WINN ET AL.

particular, we employed the red cross-disperser and used the I_2 absorption cell to calibrate the instrumental response and the wavelength scale. The slit width was $0.85''$ and the typical exposure time was 3–4 minutes, giving a resolution of about 70,000 and a signal-to-noise ratio (S/N) of approximately 200 pixel^{-1}. We observed the star for 4 hr bracketing the predicted transit midpoint and obtained a total of 56 spectra, of which 30 were taken during the transit.

We also obtained two iodine-free spectra, with a higher S/N and higher resolution. We used the sum of these spectra as a template for the Doppler analysis, which was performed with the algorithm of Butler et al. (1996). We estimated the measurement error in the Doppler shift derived from a given spectrum based on the scatter among the solutions for individual 2 Å sections of the spectrum. The typical error was 6 m s^{-1}. The data are given in Table 1 and plotted in Figures 1 and 2. Also shown in those figures are data obtained previously by O'Donovan et al. (2006), consisting of 11 velocities measured with Keck/HIRES using a different setup,[12] as well as the photometric data of Holman et al. (2007).

3. THE MODEL

To determine the projected spin-orbit angle and its uncertainty, we simultaneously fitted a parametric model to the radial velocity data, as well as the photometric data of Holman et al. (2007). We included the photometric data as a convenient way to account for the uncertainties in the photometric parameters and their covariances with the spin-orbit parameters, although in practice the photometric uncertainties were irrelevant for this system.

The model is based on a circular orbit of a star and planet. The photometric transit model was identical to the model used by Holman et al. (2007). To calculate the anomalous Doppler shift as a function of the positions of the planet and star, we used the technique of Winn et al. (2005): we simulated in-transit spectra, and determined the Doppler shifts using the same algorithm used on the actual data. The simulations rely on a template spectrum (described below) that is meant to mimic the emergent spectrum from a small portion of the photosphere. At a given moment of the transit, we denote by ϵ the fractional loss of stellar flux, and we denote by v_p the line-of-sight velocity of the occulted portion of the stellar disk. To represent the occulted portion of the stellar spectrum, we scaled the template spectrum in flux by ϵ and shifted it in velocity by v_p. We subtracted the scaled and shifted spectrum from a rotationally broadened template spectrum and then "measured" the anomalous Doppler shift Δv. This was repeated for a grid of $\{\epsilon, v_p\}$, and a polynomial function was fitted to the resulting grid. We used this polynomial to calculate the anomalous Doppler shift Δv as a function of ϵ and v_p, which are themselves functions of time. Differential rotation was ignored, as its effects are expected to be negligible (Gaudi & Winn 2007).

The template spectrum should be similar to that of TrES-2 but with slightly narrower lines because of the lack of rotational broadening. We experimented with two different empirical templates based on observations of similar stars,[13] finding that both templates gave results consistent with the function $\Delta v = -\epsilon v_p$.

---

[12] Table 3 of O'Donovan et al. (2006) gives incorrect values for the heliocentric Julian dates of the velocity measurements. The corrected dates were provided to us by D. Charbonneau (2007, private communication).

[13] The two stars were HD 38858 ($T_{\rm eff} = 5726$ K, $\log g = 4.51 \pm 0.08$, [Fe/H] $= -0.23 \pm 0.04$, $v \sin i_\star = 0.3 \pm 0.5$ km s^{-1}) and HD 66428 ($T_{\rm eff} = 5752$ K, $\log g = 4.49 \pm 0.08$, [Fe/H] $= +0.31 \pm 0.04$, $v \sin i_\star = 0.0 \pm 0.5$ km s^{-1}). The stellar parameters are from the SPOCS catalog (Valenti & Fischer 2005).

TABLE 1
RADIAL VELOCITIES OF TrES-2

HJD[a]	Radial Velocity (m s^{-1})	Measurement Uncertainty (m s^{-1})
2,454,216.96599	42.59	5.86
2,454,216.96998	38.52	5.76
2,454,216.97930	37.06	5.43
2,454,216.98973	26.69	5.76
2,454,216.99368	27.35	5.82
2,454,216.99769	21.46	5.87
2,454,217.00168	22.74	5.69
2,454,217.00564	17.82	5.75
2,454,217.00876	31.44	6.16
2,454,217.01102	16.32	6.06
2,454,217.01327	12.64	6.24
2,454,217.01552	6.15	6.05
2,454,217.01779	17.40	6.13
2,454,217.02003	19.25	6.35
2,454,217.02229	5.79	6.24
2,454,217.02453	14.41	6.35
2,454,217.02681	23.50	6.26
2,454,217.02905	6.40	6.19
2,454,217.03131	35.58	6.27
2,454,217.03356	6.90	5.92
2,454,217.03580	14.89	6.07
2,454,217.03803	16.89	6.09
2,454,217.04040	4.04	6.25
2,454,217.04266	7.37	6.17
2,454,217.04492	3.26	5.91
2,454,217.04715	0.45	6.44
2,454,217.04940	3.51	6.27
2,454,217.05165	−0.38	6.31
2,454,217.05403	2.49	6.37
2,454,217.05648	7.42	6.13
2,454,217.05907	−8.45	6.16
2,454,217.06167	−4.76	6.17
2,454,217.06425	−7.03	6.06
2,454,217.06684	−11.21	6.06
2,454,217.06957	−8.69	6.32
2,454,217.07214	−6.58	6.15
2,454,217.07473	−17.63	6.14
2,454,217.07730	−19.40	6.14
2,454,217.07991	−25.50	6.18
2,454,217.08250	−16.69	6.14
2,454,217.08513	−11.51	6.33
2,454,217.08767	−16.22	6.21
2,454,217.09031	−28.52	6.52
2,454,217.09287	−18.49	6.62
2,454,217.09545	−9.36	6.50
2,454,217.09806	−25.95	6.43
2,454,217.10065	−25.17	6.26
2,454,217.10335	−15.71	6.36
2,454,217.10608	−15.20	6.34
2,454,217.10868	−21.00	6.26
2,454,217.11124	−30.07	6.31
2,454,217.11386	−22.90	6.24
2,454,217.11709	−35.76	5.99
2,454,217.12110	−33.87	5.88
2,454,217.12509	−29.70	5.79
2,454,217.12911	−26.81	5.88

[a] Heliocentric Julian date at the photon-weighted midexposure time, i.e., weighted by the photon count rate recorded by the HIRES exposure meter.
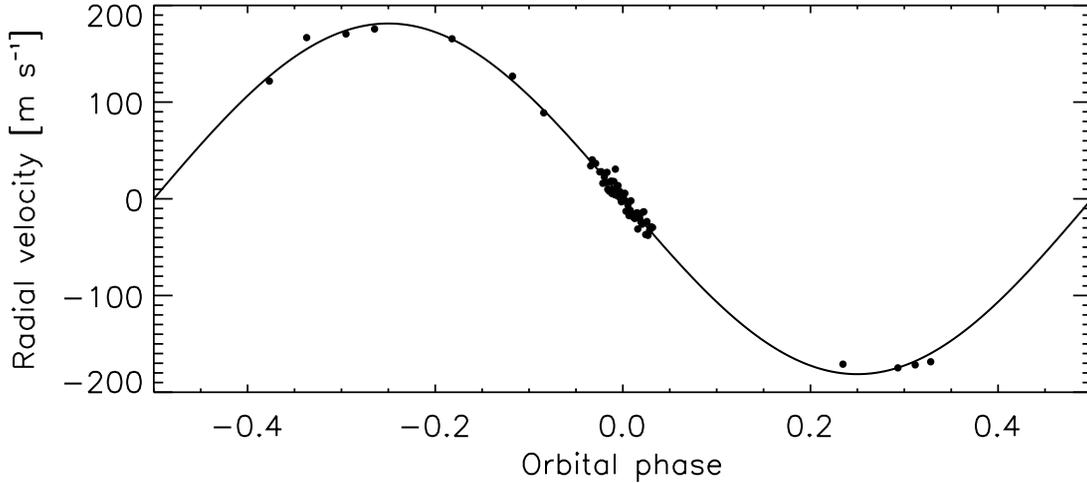
FIG. 1.—Radial velocity measurements of TrES-2, from this work and from O'Donovan et al. (2006), as a function of orbital phase. The best-fitting values of the systemic velocity have been subtracted. The solid line is the best-fitting model.
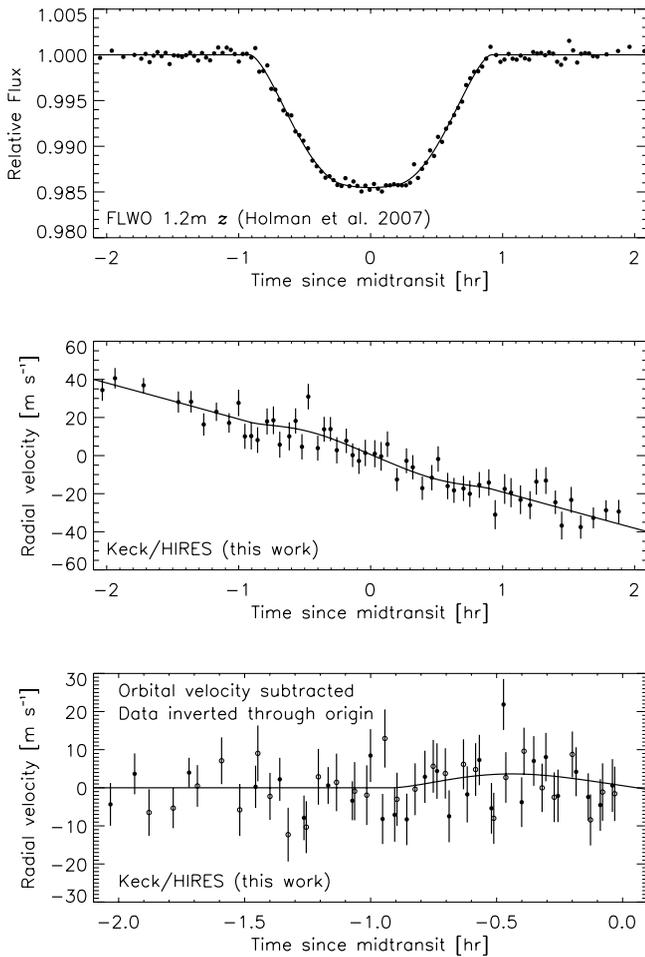

FIG. 2.— *Top*: The z-band photometry of Holman et al. (2007), averaged into 1.5 minute bins. The solid line is the best-fitting model. *Middle*: A close-up of the radial velocity data shown in Fig. 1, centered on the midtransit time. *Bottom*: Same, but the orbital velocity has been subtracted and the postmidtransit data ($t > 0$) have been inverted about the origin ($t \rightarrow -t$ and $\Delta v \rightarrow -\Delta v$), highlighting the Rossiter-McLaughlin anomaly. Filled symbols denote data from before midtransit, and open symbols denote data from after midtransit.

This function is consistent with the analytic expressions of Ohta et al. (2005) and Giménez (2006), even though those analytic expressions do not attempt to account for the spectral deconvolution. It is simpler than the quadratic or cubic functions that we have derived for other systems (Winn et al. 2005, 2006, 2007b). We do not know the reason for the difference, but it is possibly related to the much slower projected rotation speed of TrES-2.

The fitting statistic was

$$\chi^2 = \sum_{j=1}^{1033} \left[\frac{f_j(\text{obs}) - f_j(\text{calc})}{\sigma_{f,j}} \right]^2 + \sum_{j=1}^{67} \left[\frac{v_j(\text{obs}) - v_j(\text{calc})}{\sigma_{v,j}} \right]^2, \quad (1)$$

where $f_j(\text{obs})$ and $\sigma_{f,j}$ are the flux measurements and uncertainties of Holman et al. (2007), and $v_j(\text{obs})$ and $\sigma_{v,j}$ are the radial velocity measurements and uncertainties from our new data and from O'Donovan et al. (2006). The two model parameters relating to the RM effect are the line-of-sight stellar rotation velocity ($v \sin i_\star$) and the angle between the projected stellar spin axis and orbit normal (λ). The projected spin-orbit angle λ ranges from $-180°$ to $+180°$, and is measured counterclockwise on the sky from the projected stellar rotational angular momentum vector to the projected orbital angular momentum vector (see Ohta et al. 2005 or Gaudi & Winn 2007 for a diagram). If we define stellar "north" by the sky projection of the stellar angular momentum vector, then when $\lambda = 0°$ the axes are aligned and the planet moves directly "eastward" across the face of the star, for $0° < \lambda < 90°$ the planet moves "northeast," and so forth.

The other model parameters were the planetary mass (M_p), the stellar and planetary radii ($R_\star$ and R_p), the orbital inclination (i), the midtransit time (T_c), and an additive constant velocity for each of the two different velocity data sets (γ_1 and γ_2). We allowed our velocities to have a different additive constant from the velocities of O'Donovan et al. (2006) in order to account for systematic differences in the spectrograph setup and reduction procedures. We fixed the orbital period to be 2.47063 days (Holman et al. 2007). We used a Markov Chain Monte Carlo algorithm to solve for the model parameters and their confidence limits, with uniform priors on all parameters. This algorithm and our implementation of it are described in detail elsewhere (see, e.g., Winn et al. 2007a). The minimum χ^2 is 1127.6, with 1091 degrees of

TABLE 2
SYSTEM PARAMETERS OF TRES-2

Parameter	Value	68% Confidence Limits	References
P (day)	2.470621	± 0.000017	1
T_c (HJD)...	2,453,957.63479	± 0.00038	1
$(R_p/R_\star)^2$	0.0157	± 0.0003	1
$b \equiv a \cos i / R_\star$...............................	0.8540	± 0.0062	1
$M_\star$ ($M_\odot$)	0.980	± 0.062	2
$R_\star$ ($R_\odot$)	1.000	$+0.036, -0.033$	2
M_p ($M_{\rm Jup}$)....................................	1.198	± 0.053	2
R_p ($R_{\rm Jup}$)	1.220	$+0.045, -0.042$	2
$v \sin i_\star$ (km s^{-1})	1.0	± 0.6	This work
λ (deg)...	-9	± 12	This work

NOTE.—(1) Holman et al. (2007); (2) Sozzetti et al. (2007).

freedom, giving $\chi^2/N_{\rm dof} = 1.034$ and indicating an acceptable fit.

4. RESULTS

The RM effect is certainly not obvious in Figure 1, which shows the entire spectroscopic orbit. It is not even very obvious in the middle panel of Figure 2, which focuses on the velocity data around the time of transit. However, our analysis shows that the RM effect was indeed detected. As mentioned above, for the best-fitting model, $\chi^2_{\rm min} = 1127.6$. If the parameter $v \sin i_\star$ is set equal to zero, thereby neglecting the RM effect, then $\chi^2_{\rm min} = 1135.8$, with the increase of $\Delta\chi^2 = 8.2$ arising from the velocity data during the transit. We conclude that the RM effect was detected with a S/N of approximately $(8.2)^{1/2} = 2.9$. Gaudi & Winn (2007) have given analytic formulas for the S/N of RM observations as a function of the system and telescope parameters, under the assumption of Gaussian velocity errors. Using their equation (26) for this case, the forecasted S/N is 2.9, in agreement with the actual S/N.

One might wonder how much this result was influenced by the inclusion of the photometric data. To check on this, we tried setting aside the photometric data and fitting only the 67 radial velocity data points. We fixed the photometric parameters (R_p, $R_\star$, i, T_c, and P) at the values determined previously. In this case we found $\chi^2_{\rm min} = 63.7$. If $v \sin i_\star$ is set equal to zero, then $\chi^2_{\rm min} = 71.9$, giving $\Delta\chi^2 = 8.2$, just as in the full model fit. This confirms that the lowered χ^2 is an effect of a better fit to the transit velocities, and that the uncertainties in the photometric parameters are negligible in this instance.

The best-fitting model parameters are also consistent with good alignment of the spin and the orbit. Specifically, we find $\lambda = -9° \pm 12°$, and $v \sin i_\star = 1.0 \pm 0.6$ km s^{-1}, where the quoted values are the medians of the a posteriori distributions returned by the MCMC algorithm, and the error bars represent 68% confidence limits. Table 2 gives these results, along with some other relevant system parameters of TrES-2, for convenience. Visually, the RM effect is more apparent in the bottom panel of Figure 2, in which the orbital velocity has been subtracted from the data, and the sampling rate has been effectively doubled by inverting the data through the origin ($t \rightarrow -t$ and $\Delta v \rightarrow -\Delta v$). This works because for $\lambda \approx 0$, the RM waveform is antisymmetric about the origin.

Figure 3 shows the a posteriori probability distribution for λ and the joint distribution of λ and $v \sin i_\star$. The distribution for λ resembles a slightly asymmetric Gaussian function to which is added a low-level uniform probability distribution. Although only the region from $-90°$ to $+90°$ is shown in Figure 3, this low-level

uniform distribution extends all the way from $-180°$ to $+180°$. The uniform background corresponds to the very lowest allowed values of $v \sin i_\star$. This makes sense because when the rotation rate is zero, the Rossiter anomaly vanishes and λ is irrelevant. Values of λ between $-90°$ and $+90°$ correspond to prograde orbits, for which the stellar and orbital angular momenta are in the same half-plane. The integrated probability between $-90°$ and $+90°$ is 98%. We conclude that the TrES-2 orbit is prograde with 98% confidence. As an illustration of the constraints provided by our analysis, Figure 4 shows a drawing of the face of the star and the orbit of the transiting planet.

Our result for $v \sin i_\star$ is in agreement with the value reported by O'Donovan et al. (2006), 2.0 ± 1.5 km s^{-1}, which was based
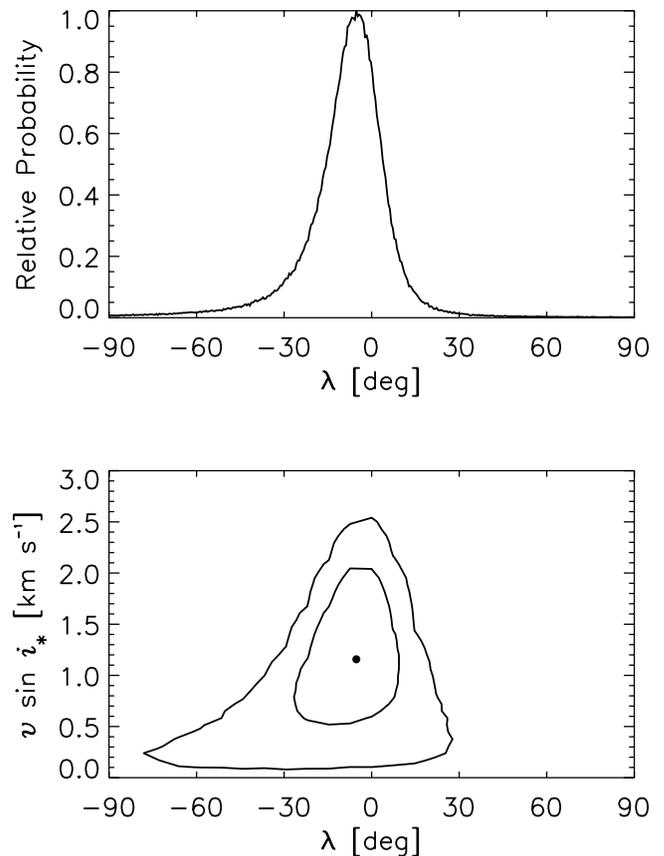

FIG. 3.—Top: Probability distribution for λ, the angle between the sky projections of the orbital axis and the stellar rotation axis. Bottom: The joint probability distribution of λ and $v \sin i_\star$. The dot shows the best-fitting values. The contours represent 68% and 95% confidence limits.
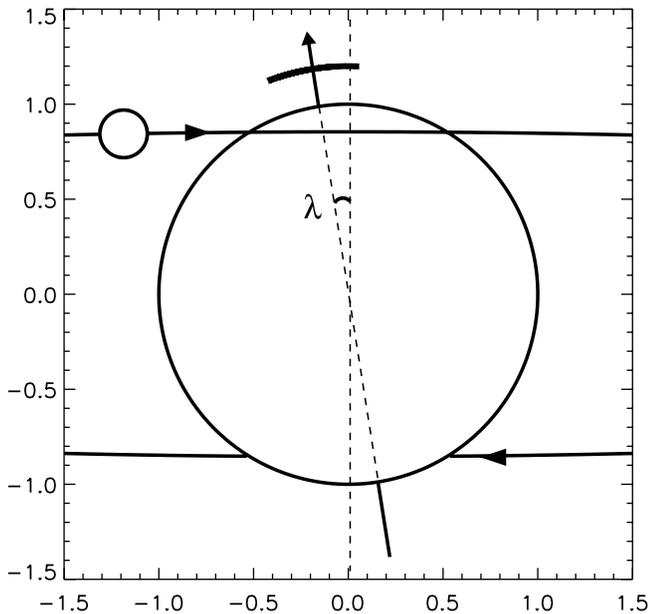
FIG. 4.— Scale drawing of the TrES-2 system. The relative radii of the bodies and the impact parameter of the transit are taken from our best-fitting model. The "north pole" of the star is drawn with an arrow, and the curved arc shows the 68% confidence region for its orientation. The angle λ is measured clockwise from the projected orbit normal vector (*vertical dashed line*) to the projected stellar north pole (*tilted dashed line*). The best-fitting value of λ is negative.

on an analysis of the line broadening in an out-of-transit spectrum. This finding is also supported by an analysis of our own out-of-transit, iodine-free spectra, using the "Spectroscopy Made Easy" (SME) software package of Valenti & Piskunov (1996). The automated analysis gave a formal result of $v \sin i_\star = 0.5 \pm 0.5$ km s^{-1}, although the true uncertainty may be larger, since with a disk-integrated spectrum of such a slow rotator it is difficult to disentangle the effects of rotation, macroturbulence, microturbulence, and the instrumental profile. In particular, the SME code assumes "typical" values for the turbulent broadening mechanisms that are of the same magnitude as the rotation speed of TrES-2 (see §§ 4.2–4.4 of Valenti & Fischer 2005).[14]

5. SUMMARY AND DISCUSSION

We have monitored the apparent Doppler shift of TrES-2 throughout a transit of its giant planet and we have detected the Rossiter-McLaughlin effect. Using the available photometric and spectroscopic data, we have found good evidence that the orbit is prograde, as are the other six systems that have been measured (with the possible exception of HD 17156), and as are the planets in the solar system. In this sense, our results for TrES-2 are not

surprising. However, as mentioned in § 1, some theories of planet migration do predict occasionally large misalignments. For example, Nagasawa et al. (2008) investigated a scenario in which a planet is scattered into an eccentric, inclined orbit with a small periastron distance (as envisioned earlier by Rasio & Ford 1996 and Marzari & Weidenschilling 2002), and subsequently a more distant planet forces Kozai oscillations in the inner planet's eccentricity and inclination. If the periastron distance is small enough during the high-eccentricity phases, the orbit may circularize at a small orbital distance with a substantial inclination. Nagasawa et al. (2008) found that this migration mechanism produces a very broad range of final inclinations, including a significant fraction of retrograde orbits. Of course, prograde orbits are also permitted in this scenario, and our finding of a prograde orbit for TrES-2 cannot be taken as evidence against this mechanism. We raise the issue only to show that a prograde orbit was not a foregone conclusion.

Furthermore, we have shown it is possible to glean this information and measure the projected spin-orbit angle to within $12°$, even for an 11th magnitude star with a slow projected rotation rate. A potentially important application of the RM effect is the detection of planets that are too small to be readily detected using other types of ground-based data. For example, in many cases of terrestrial planets detected by the *CoRoT* or *Kepler* satellites, it will be easier to observe the RM effect than to observe the star's orbital Doppler shift (and thereby measure the planet's mass). The theory underlying this idea has been discussed by Welsh et al. (2004) and Gaudi & Winn (2007).

The present work serves to illustrate this point with actual data. If TrES-2 had a rotation rate of 5 km s^{-1} instead of 1 km s^{-1}, but all other stellar and orbital parameters were the same, then the quantity and quality of data presented in this paper would permit a $\sim 3 \sigma$ detection of a planet with a radius $\sim\sqrt{5}$ times smaller than TrES-2, or ~ 6 Earth radii. If the transit were equatorial instead of grazing (the best configuration for detecting the effect, although not for assessing spin-orbit alignment), the duration of the transit would be longer by a factor of ~ 2 and the amplitude of the RM effect would be larger by a factor of ~ 2, leading to another factor-of-2 improvement in the detectable planet radius ($\sim 3 R_\oplus$). Such a planet would produce a photometric transit depth of only 8×10^{-4}, which is smaller than the transit depth of any known transiting planet.

[14] We investigated the consequences of accepting the SME result at face value, by imposing a Gaussian prior constraint on the $v \sin i_\star$ parameter with mean 0.5 km s^{-1} and standard error 0.5 km s^{-1}. In that case, the MCMC analysis gave 68%-confidence ranges of $-31°$ to $1°$ for λ and 0.3 to 1.1 km s^{-1} for $v \sin i_\star$, and showed that the orbit is prograde with 95% confidence. The constraint on λ was weakened because the SME result favors slower rotation rates, for which the sensitivity of the RM waveform to λ is reduced.

REFERENCES

Bakos, G. Á., et al. 2007, ApJ, 670, 826
Butler, R. P., Marcy, G. W., Williams, E., McCarthy, C., Dosanjh, P., & Vogt, S. S. 1996, PASP, 108, 500
Butler, R. P., et al. 2006, ApJ, 646, 505
Chatterjee, S., Ford, E. B., & Rasio, F. A. 2007, AAS DDA Meeting, 38, 1501

Fabrycky, D., & Tremaine, S. 2007, ApJ, 669, 1298
Gaudi, B. S., & Winn, J. N. 2007, ApJ, 655, 550
Giménez, A. 2006, ApJ, 650, 408
Holman, M. J., et al. 2007, ApJ, 664, 1185
Johns-Krull, C. M., et al. 2008, ApJ, 677, 657

Johnson, J. A., Marcy, G. W., Fischer, D. A., Henry, G. W., Wright, J. T., Isaacson, H., & McCarthy, C. 2006, ApJ, 652, 1724
Knutson, H. A., Charbonneau, D., Noyes, R. W., Brown, T. M., & Gilliland, R. L. 2007, ApJ, 655, 564
Loeillet, B., et al. 2008, A&A, 481, 529
Mandushev, G., et al. 2007, ApJ, 667, L195
Maness, H. L., Marcy, G. W., Ford, E. B., Hauschildt, P. H., Shreve, A. T., Basri, G. B., Butler, R. P., & Vogt, S. S. 2007, PASP, 119, 90
Marcy, G., Butler, R. P., Fischer, D., Vogt, S., Wright, J. T., Tinney, C. G., & Jones, H. R. A. 2005, Prog. Theor. Phys. Suppl., 158, 24
Marzari, F., & Weidenschilling, S. J. 2002, Icarus, 156, 570
Nagasawa, M., Ida, S., & Bessho, T. 2008, ApJ, 678, 498
Narita, N., Sato, B., Ohshima, O., & Winn, J. N. 2008, PASJ, 60, 1
Narita, N., et al. 2007, PASJ, 59, 763
O'Donovan, F. T., et al. 2006, ApJ, 651, L61
Ohta, Y., Taruya, A., & Suto, Y. 2005, ApJ, 622, 1118
Queloz, D., Eggenberger, A., Mayor, M., Perrier, C., Beuzit, J. L., Naef, D., Sivan, J. P., & Udry, S. 2000, A&A, 359, L13
Rasio, F. A., & Ford, E. B. 1996, Science, 274, 954

Sato, B., et al. 2005, ApJ, 633, 465
Sozzetti, A., Torres, G., Charbonneau, D., Latham, D. W., Holman, M. J., Winn, J. N., Laird, J. B., & O'Donovan, F. T. 2007, ApJ, 664, 1190
Torres, G., et al. 2007, ApJ, 666, L121
Udry, S., & Santos, N. C. 2007, ARA&A, 45, 397
Valenti, J. A., & Fischer, D. A. 2005, ApJS, 159, 141
Valenti, J. A., & Piskunov, N. 1996, A&AS, 118, 595
Vogt, S. S., et al. 1994, Proc. SPIE, 2198, 362
Welsh, W. F., Orosz, J. A., & Wittenmyer, R. A. 2004, BAAS, 36, 1567
Winn, J. N. 2007, in Transiting Extrasolar Planets Workshop, ed. C. Afonso, D. Weldrake, & Th. Henning, 366 (San Francisco: ASP), 170
Winn, J. N., Holman, M. J., & Fuentes, C. I. 2007a, AJ, 133, 11
———. 2005, ApJ, 631, 1215
———. 2006, ApJ, 653, L69
———. 2007b, ApJ, 665, L167
Wolf, A. S., Laughlin, G., Henry, G. W., Fischer, D. A., Marcy, G., Butler, P., & Vogt, S. 2007, ApJ, 667, 549
Wu, Y., Murray, N. W., & Ramsahai, J. M. 2007, ApJ, 670, 820